CHIN. PHYS. LETT. Vol. 38, No. 12 (2021) 128701

Edge Transport and Self-Assembly of Passive Objects in a Chiral Active Fluid

Qing Yang(杨庆)[1,2], Huan Liang(梁欢)[1,2], Rui Liu(刘锐)[1], Ke Chen(陈科)[1,2,3], Fangfu Ye(叶方富)[1,2,3,4*], and Mingcheng Yang(杨明成)[1,2,3*]

[1]*Beijing National Laboratory for Condensed Matter Physics and Laboratory of Soft Matter Physics, Institute of Physics, Chinese Academy of Sciences, Beijing 100190, China*
[2]*School of Physical Sciences, University of Chinese Academy of Sciences, Beijing 100049, China*
[3]*Songshan Lake Materials Laboratory, Dongguan 523808, China*
[4]*Wenzhou Institute, University of Chinese Academy of Sciences, Wenzhou 325001, China*

(Received 8 October 2021; accepted 12 November 2021; published online 8 December 2021)

Topological edge flow and dissipationless odd viscosity are two remarkable features of chiral active fluids composed of active spinners. These features can significantly influence the dynamics of suspended passive particles and the interactions between the particles. By computer simulations, we investigate the transport phenomenon of anisotropic passive objects and the self-assembly behavior of passive spherical particles in the active spinner fluid. It is found that in confined systems, nonspherical passive objects can stably cling to boundary walls and are unidirectionally and robustly transported by edge flow of spinners. Furthermore, in an unconfined system, passive spherical particles are able to form stable clusters that spontaneously and unidirectionally rotate as a whole. In these phenomena, strong particle-wall and interparticle effective attractions play a vital role, which originate from spinner-mediated depletion-like interactions and can be largely enhanced by odd viscosity of spinner fluids. Our results thus provide new insight into the robust transport of cargoes and the nonequilibrium self-assembly of passive intruders.

DOI: 10.1088/0256-307X/38/12/128701

Active matter consists of self-driven units, of which each can transform stored or ambient free energy into its motility and is intrinsically out of equilibrium.[1,2] Active matters are ubiquitous in nature and can also been easily realized in experiments, ranging from living biological organisms to artificial self-propelled colloids and granular systems.[3–5] Among active systems, chiral active fluids composed of interacting active spinners constitute an important class, which break both time-reversal and parity symmetries. Chiral active fluids often exhibit exotic phenomena, such as the spontaneous unidirectional edge flow[6–10] or novel phase behaviors,[11–14] and have currently attracted considerable interests.

Recently, Dasbiswas *et al.* have proven that a one-way edge flow of a spinner fluid is topologically protected and thus is immune to disorder and defect at the system boundaries.[10] Such a topological edge mode, originally discovered in electronic quantum Hall states,[15–22] could provide robust channels for transport of material and information. Moreover, the chiral active fluid is shown to have a non-dissipative transport coefficient called odd viscosity,[23] which arises from breaking of time-reversal symmetry and is usually discussed in quantum Hall fluids.[24] When shearing the fluid in one direction, the odd viscosity induces a momentum transfer in the perpendicular direction. The odd viscosity of the chiral active fluid depends on the spinner activity (being an odd function of the spinner chirality), and can markedly affect the dynamic behavior of the fluid.[8,25–31] In a recent work, we demonstrated that a combination of the edge flow and odd viscosity of the spinner fluid can lead to a strong depletion-like attraction between an immersed spherical passive object and the system boundary, which is dependent on the spinner activity. With the tunable effective attraction, a passive object can stably cling to the boundary and be unidirectionally entrained by the edge flow of the spinner fluid. Consequently, the spherical intruder can be topologically transported along the system boundary in a controllable manner.[32] These findings not only provide new design principles for cargo transport in complex fluid environment, but also suggest new possibilities to regulate the effective force on immersed passive objects.

In the previous study, the intruder transported topologically along the system boundary was an isotropic spherical particle. Thus, a very natural question deserved further study is whether a nonspherical intruder with anisotropic geometric structure can be transported in a similar way. Moreover, another in-

Supported by the National Natural Science Foundation of China (Grant Nos. 11874397, 11774393, 11774394, and 11974044), and the Strategic Priority Research Program of Chinese Academy of Sciences (Grant No. XDB33030300).
*Corresponding authors. Email: fye@iphy.ac.cn; mcyang@iphy.ac.cn
© 2021 Chinese Physical Society and IOP Publishing Ltd

teresting question, inspired by the spinner-mediated depletion-like interaction between the passive intruder and the boundary, is whether there also exists an odd viscosity-dependent effective attraction between the passive intruders immersed in the chiral active fluid. If any, could this *in situ* adjustable effective interaction be used to flexibly direct the self-assembly of immersed passive objects? Although the effective interactions between passive particles mediated by active bath and the resulting self-assembly have been extensively investigated,[33–41] the self-assembly induced due to the odd viscosity-enhanced depletion-like interaction has not yet been discussed so far.

In this Letter, we address the above two questions by means of computer simulations. Firstly, we investigate the feasibility of transporting the non-spherical cargoes via the edge flow of chiral active fluid in a confined system. We find that nonspherical passive intruders, including square, triangular and rod-like objects, stably stay close to the system boundary and are unidirectionally entrained along the boundary. The transport velocity and the dwelling probability of the intruder at the boundary can be adjusted by varying the spinner activity. Secondly, we study the self-assembly of large passive spheres in the spinner fluid under periodic boundary conditions. The spherical particles can form stable clusters that exhibit a spontaneous and unidirectional rotation. The cluster size significantly hinges on the activity and packing fraction of the spinners and the concentration of the passive spheres. All the results can be reasonably understood based on the edge flow and the odd viscosity-dependent depletion-like attraction.

Simulation System—Edge Transport of Nonspherical Cargo. The system is composed of a collection of active spinners and a passive nonspherical intruder, which are confined in a circular boundary of radius $R_{\rm w} = 41$, as shown in Fig. 1(b). Here, each spinner is modeled as a 2D disk with diameter $\sigma_{\rm s} = 2$, and the nonspherical intruder is constructed by rigidly linking disks of diameter $\sigma_{\rm s} = 2$ according to the prescribed shape, as sketched in Figs. 1(a), 1(c) and 1(e), corresponding to the square, triangular and rod-like intruders, respectively. The spinner-spinner and spinner-wall interactions via a repulsive Lennard–Jones (LJ) type of potential can be expressed by

$$U(r) = 4\epsilon\left[\left(\frac{\sigma_{\rm s}}{r}\right)^{2n} - \left(\frac{\sigma_{\rm s}}{r}\right)^{n}\right] + \epsilon, \quad r < 2^{1/n}\sigma_{\rm s},$$

where the potential stiffness $n = 12$ for the former and $n = 24$ for the latter. Besides the steric potential interaction, different spinners also couple tangentially via a bounce-back collision rule, which generates a tangential friction between spinners.[32] The dynamics of the active spinners evolves according to the underdamped Langevin equation:

$$m_{\rm s}\dot{\boldsymbol{v}}_{\rm s} = -\gamma_{\rm s}\boldsymbol{v}_{\rm s} + \boldsymbol{F}(r) + \boldsymbol{\zeta}, \tag{1}$$

$$I_{\rm s}\dot{\omega}_{\rm s} = -\gamma_r\omega_{\rm s} + T_{\rm d} + \xi, \tag{2}$$

with $m_{\rm s} = 1$ being the mass of the spinner, $I_{\rm s} = 0.5$ the moment of inertia, $\gamma_{\rm s} = 100$ and $\gamma_r = \frac{1}{3}\sigma_{\rm s}^2\gamma_{\rm s}$ the translational and rotational friction coefficients, respectively. Here, $\boldsymbol{F}(r)$ includes the interparticle or particle-wall potential interactions, $T_{\rm d}$ refers to the driving torque on the spinner, and $\boldsymbol{\zeta}$ to the Gaussian-distributed stochastic force with $\langle\boldsymbol{\zeta}(t)\rangle = 0$ and $\langle\zeta_i(t)\zeta_j(t')\rangle = 2k_{\rm B}T\gamma_{\rm s}\delta_{ij}\delta(t-t')$, and ξ to the Gaussian-distributed stochastic torque with zero mean and $\langle\xi(t)\xi(t')\rangle = 2k_{\rm B}T\gamma_r\delta(t-t')$. In the simulation, the temperature is taken as $k_{\rm B}T = 0.8\epsilon$ with $k_{\rm B}$ the Boltzmann constant, and the packing fraction of the spinner is fixed at $\rho = 0.6$.

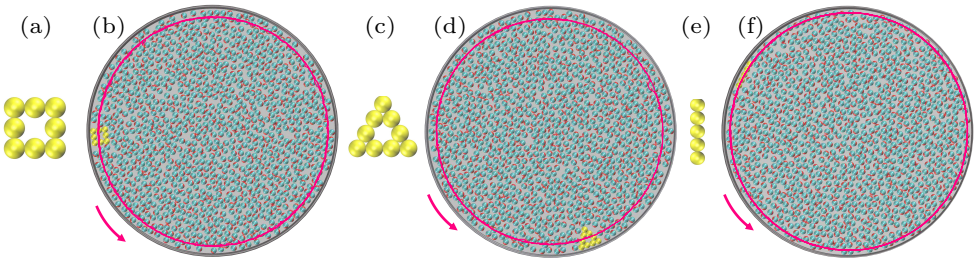

Fig. 1. Sketches of (a) square, (c) triangular, and (e) rod-like intruders constructed by rigidly linking smooth beads. [(b), (d), (f)] Corresponding to the simulation snapshots of the square, triangular, and rod-like intruders, respectively, transported along the system boundary for several rounds in the active spinner fluid. The pink arrows mark the direction of the edge transport, and the pink lines represent the trajectories of intruders which are stably transported along the boundary. In (b), (d) and (f), the driving torque $T_{\rm d} = 30$ is used and the packing fraction of the spinner is fixed at $\rho = 0.6$.

On the other hand, the dynamics of the rigid passive intruder obeys the similar underdamped Langevin equations, but without the driving torque ($T_{\rm d} = 0$). As the passive intruder has an anisotropic shape, besides the translation of its center of mass, its orientation may also experience a rotational motion. Here, the constituent disks of the intruder are frictionless, and they interact with the spinners and the wall

through the same repulsive LJ potential. In order to reduce the translational and rotational relaxation time of the passive intruder, the translational and rotational friction coefficients are, respectively, taken as $\gamma_{\rm p} = \gamma_{\rm s}$ and $\gamma_r' = 12\gamma_r$.

Self-Assembly of Spherical Intruders. To study the self-assembly behavior of the passive intruders induced by the active spinners, a few passive spherical intruders are dispersed in a chiral active fluid. The simulation system has dimensions of $L_x = L_y = 60$, under the periodic boundary conditions in both directions. The passive intruder is modeled as a large frictionless disk, which interacts with the nearby intruders and spinners via the same repulsive LJ potential, as described above. In the simulations, the packing fraction of spinners is taken as $\rho \simeq 0.6$, and the system temperature as $k_{\rm B}T = 0.8$, the intruder diameter as $\sigma_{\rm p} = 4\sigma_{\rm s}$ and the intruder translational friction coefficient as $\gamma_{\rm p} = \gamma_{\rm s}$, unless stated otherwise.

Results and Discussion—Edge Transport of Nonspherical Cargo. To study the feasibility of the edge transport of the nonspherical intruders, the intruders are initially placed near the center of the active spinners fluid with a moderate activity. After experiencing a diffusion process, all the intruders stably cling to the confinement boundary and are unidirectionally entrained by the edge flow of the spinners, as shown in the Supplementary Materials (see Movie S1 in the Supplementary Materials). Figures 1(b), 1(d) and 1(f) display, respectively, the trajectories of the square, triangular and rod-like intruders that experience a stable unidirectional edge transport along the system boundary without fixed obstacle, with the intruder centers close to the boundary, similar to the edge transport behavior of a spherical cargo.[32] When there exists an obstacle fixed at the system boundary, the intruder can still experience a stable edge transport (see Movie S2–S4 in the Supplementary Materials). The transport direction is counterclockwise, as the edge flow of the active spinner fluid is counterclockwise. These results indicate that the edge transport is quite robust, insensitive to the intruder and boundary shape.

From the simulations we compute the dwelling probability Pr of the intruder staying at the boundary and the transport velocity for different driving torques. A stable transport along the system boundary occurs when the dwelling probability of cargo is close to 1. As depicted in Figs. 2(a)–2(c), the dwelling probabilities of all the intruders increase with the driving torque and approach to 1 around $T_{\rm d} = 20$. The increase of the dwelling probability with $T_{\rm d}$ arises from the fact that the effective depletion attraction between the intruders and boundary mediated by the spinners (depletant) enhances with increasing $T_{\rm d}$, as the case of spherical cargo studied in our previous work.[32] This also implies that the equilibrium depletion attraction[42] induced by the passive depletants is not sufficient to achieve a stable edge transport ($Pr \ll 1$). In Ref. [32], we have shown that the enhancement of the effective depletion attraction results from the joint effect of the edge flow and odd viscosity of the spinner fluid. Briefly, in the nonequilibrium chiral active fluid, the depletion interaction between the intruder and the boundary is proportional to the normal stress on the intruder surface, $-\sigma_{\rm nn}A_{\rm e}$, with $A_{\rm e}$ being the effective collision cross section of the intruder. According to the hydrodynamic theory of the chiral active fluid,[23,32] the steady-state normal stress of the spinner fluid can be calculated by

$$\sigma_{\rm nn} = -p_0 - 2\eta_{\rm o} v_\varphi / R, \tag{3}$$

where p_0 is the hydrostatic pressure, R the characteristic size of the intruder, v_φ the tangential velocity of the spinner edge flow around the intruder, and $\eta_{\rm o}$ refers to the odd viscosity of the active spinner fluid.

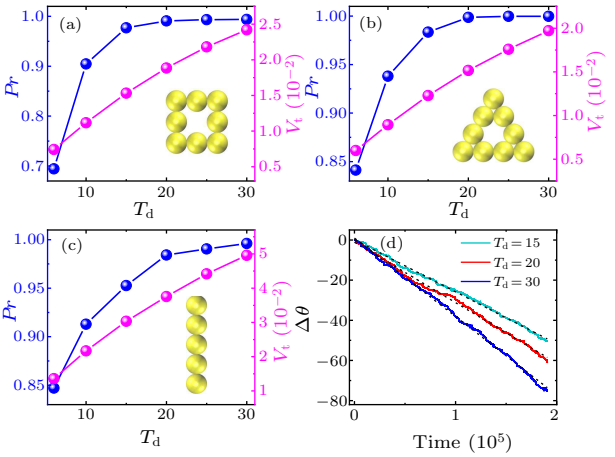

Fig. 2. Dwelling probability (blue circle, left longitudinal axis) and transport velocity (magenta circle, right longitudinal axis) of (a) square, (b) triangular and (c) rod-like intruders as a function of the driving torque. (d) The angular displacement of the self-assembled structure of three passive intruders (Fig. 3) as a function of time for different driving torques. The dashed lines are linear fittings to the simulation measurement, yielding the angular velocity -2.59×10^{-4}, -3.01×10^{-4} and -3.91×10^{-4} for $T_{\rm d} = 15$, 20 and 30, respectively.

Equation (3) indicates that besides the pressure, the odd viscosity together with the edge flow also contribute to the normal stress, absent in conventional fluids. The odd viscosity and edge flow velocity both increase with the spinner activity,[32] such that the effective depletion attraction on the intruder mediated by the spinners, hence Pr, enhances as the driving torque increases ($\eta_{\rm o} v_\varphi > 0$). When the activity vanishes (equilibrium fluid), only the pressure contributes to the depletion force. Among the three nonspherical cargoes, the dwelling probability of the square cargo is slightly lower (0.7) at a low torque, as displayed in

Fig. 2(a). This is due to the fact that the square intruder has the smallest collision section (namely side length), thus the weakest depletion attraction.

Further, Fig. 2 shows that the transport velocities of all the intruders grow almost linearly with the driving torque, as the edge flow velocity entraining the intruder is directly proportional to the spinner activity.[32] Among these cargoes, the transport velocity of the rod-like cargo is largest and that of the triangle cargo is smallest. This can be understood based on the fact that during the steady-state transport the center of the rod-like cargo is closest to the boundary wall, while that of the triangular cargo is farthest from the boundary. The edge flow velocity decays sharply from the boundary wall, so different intruders experience different local flow velocities.

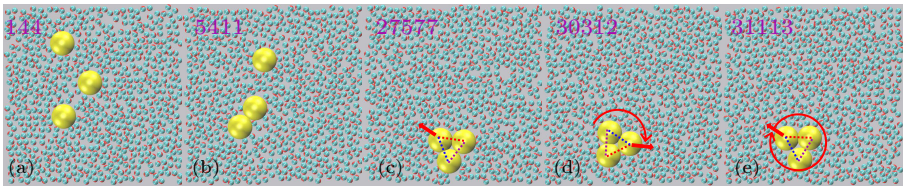

Fig. 3. (a)–(e) Snapshots of the intruders (yellow beads) assembled into a triangular cluster, rotating clockwise around its center. The numbers show the scaled time in the simulation. The straight arrow marks the orientation of the triangular structure, and the curved arrow denotes the direction of its rotation. Here, the torque is taken as $T_{\rm d} = 30$.

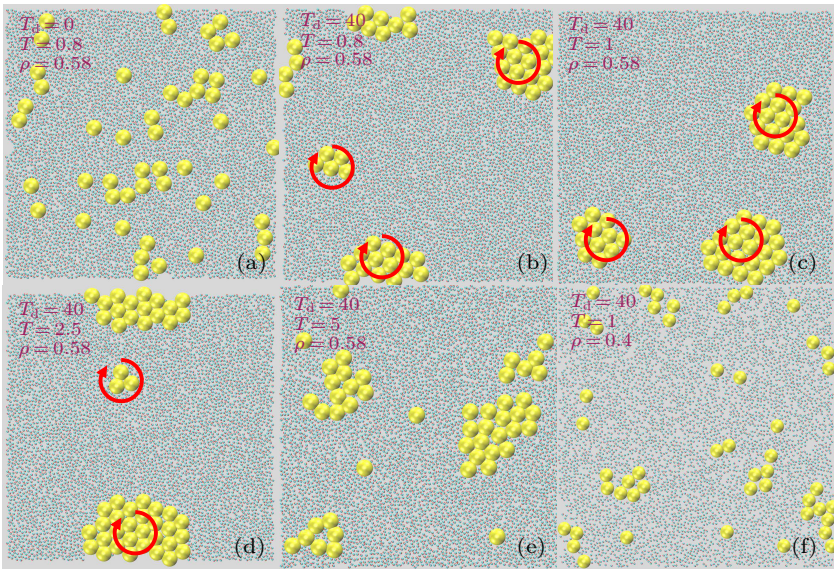

Fig. 4. (a)–(f) Self-assembled structures of passive intruders under different conditions marked on the top-left corner of each subgraph. The red curve arrows represent the rotating direction of the assembled clusters. Here, $\sigma_{\rm p} = 5\sigma_{\rm s}$ is used to enhance the effective depletion-like attraction, and all the patterns are obtained in the same number of simulation steps.

In brief, the topological edge flow of the spinner fluid still can unidirectionally transport immersed nonspherical intruders along the system boundary, which is quite robust and insensitive to the intruder shape. The transport behavior of the nonspherical cargoes in the spinner fluid can be explained in the same way as the situation of spherical cargo.

Self-Assembling into Rotating Clusters of Spherical Intruders. So far, we have realized that the spinners are able to induce an activity-dependent depletion attraction between the intruder and the boundary wall, and we can predict that similar effective attraction should also exists between the immersed intruders, resulting in their self-assembly. Firstly, we study the possible self-assembling behavior of three immersed passive intruders. It is found that these intruders can spontaneously form a rigidly rotating trimer. As illustrated in Fig. 3, at the beginning, the nearest neighbor intruders form a dimer, moving together and rotating unidirectionally around its center. After undergoing a long diffusion, the dimer incorporates another intruder, and assembles into a stable trimer, namely a regular triangular structure. The self-assembled trimer diffuses translationally and rotates clockwise around its center as a whole, as displayed in the Supplementary Materials (Movie S5). The unidirectional rotation of the trimer results from the drag on the trimer exerted by the surrounding spinner edge flow. Note that at the internal boundary (trimer surface) the spinner (counterclockwise spinning) edge flow is clockwise,[32] opposite to the case of the external confinement boundary in Fig. 1. Fig-

ure 2(d) reveals that the rotating angular velocity of the self-assembled trimer increases with the driving torque, as is expected. Compared to the equilibrium depletant-induced self-assembly of large objects, the present self-assembled structure experiences a unidirectional rotation, and its binding affinity is *in situ* tunable by changing the spinner activity.

To further explore such self-assemble behavior, more intruders are placed in the spinner fluid, as displayed in Fig. 4. When $T_{\rm d} = 0$ (passive depletant), no stable cluster emerges [Fig. 4(a)] and apparently there is only a weak attraction between the intruders contributed by the equilibrium depletion effect. For a large activity such as $T_{\rm d} = 40$, the diffusing intruders aggregate together, gradually forming dimers, trimers, and larger clusters, which spontaneously and unidirectionally rotate around their centers [Fig. 4(b)]. The results further confirm that the self-assembling effect mainly stems from the odd viscosity-induced depletion-like interaction due to the active spinning.

Figures 4(b)–4(f) show the cluster formation from the intruders under different conditions. The simulation results indicate that there exists an optimal temperature range for the clustering capability of the intruders, around $T = 2.5$ [Fig. 4(d) and Movie S6 in the Supplementary Materials], which may be explained directly as follows. In the low-temperature regime, the intruders diffuse too slowly to frequently meet each other (i.e., locate within the effective range of the depletion attraction). A high temperature promotes the intruder diffusion and the interparticle collision frequency although the thermal fluctuations are sufficiently intense to easily destabilize and destroy the intruder clusters [see Fig. 4(e) with the temperature $T = 5$]. Moreover, the intruder cluster is difficult to form when lowering the packing fraction of the spinner fluid ($\rho = 0.4$) and keeping other parameters unchanged, as shown in Fig. 4(f). This indicates that the depletion-like attraction between the intruders for $\rho = 0.4$ does not sufficiently overwhelm the thermal fluctuation so as to stabilize the cluster structure, which is consistent with the fact that both pressure and odd-viscosity contributions to the normal stress [Eq. (3)] reduce with decreasing the spinner packing fraction.

The above results unambiguously demonstrate that the active spinner mediated depletion interaction, which can be greatly enhanced due to the odd viscosity of the spinner fluid, can give rise to a self-assembly of the immersed passive intruders. It could be expected that the intruders will finally form a 2D hexagonal crystal, when the number of intruders is large enough and the simulation time is long enough.

In summary, we have demonstrated by simulation that, using the odd-viscosity-enhanced depletion-like interactions, the topological edge flow of the chiral active fluid can robustly transport the nonspherical passive intruders, including the square, triangular and rod-like objects. The transport behavior is controllable by tuning the spinner activity. The present work generalizes our previous study on the topological edge transport of isotropic cargo. We show that the odd-viscosity-enhanced effective attractions can cause the immersed passive intruders to self-assemble into unidirectionally rotating clusters. The size and rotational velocity of the intruder cluster can be *in situ* adjusted by changing the driving torque on the spinners. There appears an interesting and open question whether dynamically changing the spinner activity may promote or even realize a targetable self-assembly of passive intruders. Moreover, obtaining a phase diagram of the passive intruders in the spinner fluid in a wide range of parameter space deserves further study, which will be addressed in our future work. Our findings provide a new possibility to employ the active spinner fluid to robustly transport cargoes in complex fluid environment and to direct the self-assembly of immersed intruders.

References

[1] Marchetti M C, Joanny J F, Ramaswamy S, Liverpool T B, Prost J, Rao M and Simha R A 2013 *Rev. Mod. Phys.* **85** 1143
[2] Das M, Schmidt C F and Murrell M 2020 *Soft Matter* **16** 7185
[3] Ramaswamy S 2010 *Annu. Rev. Condens. Matter Phys.* **1** 323
[4] Vicsek T and Zafeiris A 2012 *Phys. Rep.* **517** 71
[5] Zhou A, Qiao L Y, Wei G N, Jiang Z T and Zhao Y H 2020 *Chin. Phys. Lett.* **37** 050501
[6] Tsai J C, Ye F, Rodriguez J, Gollub J P and Lubensky T C 2005 *Phys. Rev. Lett.* **94** 214301
[7] Liu P, Zhu H, Zeng Y, Du G, Ning L, Wang D, Chen K, Lu Y, Zheng N, Ye F and Yang M 2020 *Proc. Natl. Acad. Sci. USA* **117** 11901
[8] Soni V, Bililign E S, Magkiriadou S, Sacanna S, Bartolo D, Shelley M J and Irvine W T 2019 *Nat. Phys.* **15** 1188
[9] Yang X, Ren C, Cheng K and Zhang H P 2019 *Phys. Rev. E* **101** 022603
[10] Dasbiswas K, Mandadapu K K and Vaikuntanathan S 2018 *Proc. Natl. Acad. Sci. USA* **115**
[11] Nguyen N, Klotsa D, Engel M and Glotzer S C 2014 *Phys. Rev. Lett.* **112** 075701
[12] Yeo K, Lushi E and Vlahovska P M 2015 *Phys. Rev. Lett.* **114** 188301
[13] Grzybowski B A and Whitesides G M 2002 *Science* **296** 718
[14] Huang Z F, Menzel A M and Löwen H 2020 *Phys. Rev. Lett.* **125** 218002
[15] Klitzing K V, Dorda G and Pepper M 1980 *Phys. Rev. Lett.* **45** 494
[16] Thouless D J, Kohmoto M, Nightingale M P and den Nijs M 1982 *Phys. Rev. Lett.* **49** 405
[17] Haldane F D M 1988 *Phys. Rev. Lett.* **61** 2015
[18] Kane C L and Mele E J 2005 *Phys. Rev. Lett.* **95** 226801
[19] Bernevig B A, Hughes T L and Zhang S C 2006 *Science* **314** 1757
[20] Qi X L and Zhang S C 2010 *Rev. Mod. Phys.* **83** 1057
[21] Hasan M Z and Kane C L 2010 *Rev. Mod. Phys.* **82** 3045

[22] Liu R Z, Huang X, Zhao L X, Liu L M, Yin J X, Wu R, Chen G F, Wang Z Q and Pan S H 2019 *Chin. Phys. Lett.* **36** 117301
[23] Banerjee D, Souslov A, Abanov A G and Vitelli V 2017 *Nat. Commun.* **8** 1
[24] Avron J, Seiler R and Zograf P G 1995 *Phys. Rev. Lett.* **75** 697
[25] Lapa M F and Hughes T L 2014 *Phys. Rev. E* **89** 043019
[26] Kogan E 2016 *Phys. Rev. E* **94** 043111
[27] Souslov A, Dasbiswas K, Fruchart M, Vaikuntanathan S and Vitelli V 2019 *Phys. Rev. Lett.* **122** 128001
[28] Abanov A, Can T and Ganeshan S 2018 *SciPost Phys.* **5** 010
[29] Bao G and Jian Y 2021 *Phys. Rev. E* **103** 013104
[30] Hosaka Y, Komura S and Andelman D 2021 *Phys. Rev. E* **103** 042610
[31] Hosaka Y, Komura S and Andelman D 2021 arXiv:2109.02321 [cond-mat.soft]
[32] Yang Q, Zhu H, Liu P, Liu R, Shi Q, Chen K, Zheng N, Ye F and Yang M 2021 *Phys. Rev. Lett.* **126** 198001
[33] Dolai P, Simha A and Mishra S 2018 *Soft Matter* **14** 6137
[34] Angelani L 2019 *J. Phys. Condens. Matter* **31** 075101
[35] Takatori S C and Brady J F 2015 *Soft Matter* **11** 7920
[36] Ma Z, Lei Q L and Ni R 2017 *Soft Matter* **13** 8940
[37] Wang Y, Shen Z, Xia Y, Feng G and Tian W 2020 *Chin. Phys. B* **29** 053103
[38] Singh D P, Choudhury U, Fischer P and Mark A G 2017 *Adv. Mater.* **29** 1701328
[39] Stenhammar J, Wittkowski R, Marenduzzo D and Cates M E 2015 *Phys. Rev. Lett.* **114** 018301
[40] Smrek J and Kremer K 2017 *Phys. Rev. Lett.* **118** 098002
[41] Alaimo F and Voigt A 2018 *Phys. Rev. E* **98** 032605
[42] Asakura S and Oosawa F 1954 *J. Chem. Phys.* **22** 1255